Alzheimer's
Research & Therapy

RESEARCH

Open Access

Toward a more comprehensive understanding of network centrality disruption in amnestic mild cognitive impairment: a MEG multilayer approach

Ignacio Taguas[1,2*], Sandra Doval[1,3], Fernando Maestú[1,3,4*] and David López-Sanz[1,3]

Abstract

Background Alzheimer's Disease (AD) is the most common form of dementia. Its early stage, amnestic Mild Cognitive Impairment (aMCI), is characterized by disrupted information flow in the brain. Previous studies have yielded inconsistent results when using electrophysiological techniques to investigate functional connectivity changes in AD, and a contributing factor may be the study of brain activity divided into frequencies.

Methods Our study aimed to address this issue by employing a cross-frequency approach to compare the functional networks of 172 healthy subjects and 105 aMCI patients. Using magnetoencephalography, we constructed source-based multilayer graphs considering both intra- and inter-frequency functional connectivity. We then assessed changes in network organization through three centrality measures, and combined them into a unified centrality score to provide a comprehensive assessment of centrality disruption in aMCI.

Results The results revealed a noteworthy shift in centrality distribution in aMCI patients, both in terms of spatial distribution and frequency. Posterior brain regions decrease synchrony between their high-frequency oscillations and other regions' activity across all frequencies, while anterior regions increase synchrony between their low-frequency oscillations and other regions' activity across all frequencies. Thus, posterior regions reduce their relative importance in favor of anterior regions.

Conclusions Our findings provide valuable insights into the intricate changes that occur in functional brain networks during the early stages of AD, demonstrating that considering the interplays between different frequency bands enhances our understanding of AD network dynamics and setting a precedent for the study of functional networks using a multilayer approach.

Keywords Alzheimer's disease, Graph theory, Multilayer networks, Functional connectivity, MEG

*Correspondence:
Ignacio Taguas
itaguas@ucm.es
Fernando Maestú
fmaestuu@ucm.es
Full list of author information is available at the end of the article

Background

Alzheimer's Disease (AD) is an incurable neurodegenerative disease that accounts for about two-thirds of dementia cases [1]. The clinical manifestations start with a progressive loss of episodic memory, followed by impairment of other cognitive domains [2]. But clinical symptoms are only the tip of the iceberg, as they appear ten to fifteen years after the earliest neuronal dysfunctions occur [3]. The cascade of events leading to AD starts with the malfunctioning of two key proteins, amyloid-β (Aβ) and tau, which accumulate to form extracellular Aβ plaques and intracellular tau neurofibrillary tangles. These aggregates affect synapses, altering neuronal communication, and as more synapses disappear, functional networks are disrupted, ultimately causing cognitive dysfunctions. Thus, brain network disruption constitutes a potential marker for the detection of AD even before clinical symptoms manifest, and its study in the early stages of the disease is crucial.

Mild cognitive impairment (MCI) is generally considered the prodromal stage of AD. MCI represents a stage of cognitive decline that is more severe than typical age-related changes, but not as pronounced as the cognitive decline seen in AD [4]. MCI is a clinical state characterized by a decline in cognition not severe enough to affect independence in everyday activities. Its most common subtype, amnestic MCI (aMCI), conveys memory impairment, and is more likely to progress to AD [5].

Electrophysiology provides a non-invasive and accessible means to study brain function in AD and MCI. In particular, previous studies using magnetoencephalography (MEG) have offered valuable insights for diagnosis and understanding disease mechanisms (e.g., [6–8]; see [8] for a review). Brain networks are commonly studied through functional connectivity: the statistical dependence through time between physiological signals from different brain regions [9]. Functional connectivity is a direct measure of brain synchrony. Increments in functional connectivity reflect an increase in brain synchrony, while decreases imply the opposite; both changes can be pathological.

Functional connectivity disruption in AD and aMCI patients is a common finding. However, previous literature shows erratic results due to conflicting methodological factors (including differences in the various functional connectivity metrics, inconsistencies in diagnostic criteria, and inadequacies in sample sizes) [10]. Here, we review the most persistent results. The anterior aspects of the brain exhibit hypersynchrony in patients in delta and theta frequencies [11, 12], and sometimes in alpha [13]. The posterior aspects of the brain exhibit hyposynchrony in patients in alpha and beta [14, 15], and seldom in gamma [16]. In the earliest (preclinical) stages of the disease, studies report hypersynchrony in theta and delta in posterior brain regions [17].

Functional connectivity analyses involve examining pairwise correlations, providing information on how strongly different brain regions are connected. A further step in the study of functional networks is modeling them as graphs. A graph is a set of elements, called nodes, connected by links. Under this framework, nodes denote brain regions and links denote functional connectivity values. This framework allows us to study how changes in functional connectivity affect global network parameters, such as information flow and integration [18].

One of the main advantages of graphs is that they allow us to study the importance of each neural substrate in the network by measuring their centrality. In graph theory, centrality is a measure of the role each node plays in the graph, offering insights into how specific nodes contribute to network structure and how their impairment could affect the network. There are multiple metrics that quantify the centrality of a network node, each considering different aspects of how information flows on a network [19]. For this reason, authors suggest that aggregating rankings across multiple measures might yield more robust centrality results [19, 20].

Analyses using graph theory imply a greater level of abstraction and methodological complexity than those directly measuring functional connectivity, which further complicates the interpretation of the results. Consequently, existing papers reach even more conflicting conclusions (for reviewing the state of the art, see [21, 22]). Even so, it is a common finding that variations in cerebrospinal fluid biomarkers, namely Aβ and tau, entail centrality changes in aMCI and AD [12, 23].

All the articles mentioned in the previous paragraphs treat the different frequency bands individually. Separating brain signals into discrete and isolated frequency bands is convenient, as each band has been associated with specific physiological processes. Nonetheless, this strict division represents an oversimplification of brain dynamics. Several authors suggest that studying frequency-specific functional graphs in isolation might play a role in the dissimilar results between studies and hint at the use of a more integrative approach: the use of multilayer graphs, in which each layer corresponds to a frequency band. These graphs consider the interplays between the different frequency bands, as they contain both intra- and inter-band connections. In a recent study, Yu et al. (2017) concluded that MEG-based brain graphs comprising all bands reveal information that cannot be extracted by studying the frequency graphs separately, although this work solely focused on intra-band connections.

While several studies have demonstrated the usefulness of applying a graph-multilayer approach, few have investigated centrality disruption in different brain disorders; examples can be found for AD [24] and schizophrenia [25], but not MCI. In the present work, we have approached centrality changes, measured by several widely used centrality metrics, in aMCI patients, considering functional connectivity interactions between all pairs of nodes in all frequency bands. To prevent oversimplifying the network structure, we constructed the graphs using brain sources as nodes and the original functional connectivity values as links, without applying any transformations (such as thresholding or binarization). We expect aMCI participants to exhibit centrality disruptions affecting their whole brain communication patterns. Since previous studies suggest non-linear trajectories during AD, we anticipate both centrality increases and decreases depending on the brain region.

Materials and methods

Participants

The study participants were recruited from three different locations in Madrid, Spain: Hospital Clínico San Carlos, Centro de Prevención del Deterioro Cognitivo, and Centro de Mayores del Distrito de Chamartin. The sample comprised 277 participants: 172 healthy controls aged 60–82 (105 women) and 105 aMCI patients aged 64–85 (69 women). Table 1 summarizes the most important demographic and neuropsychological characteristics.

To assess the general cognitive and functional status of each participant, a group of experts consisting of neuropsychologists, psychiatrists, and neurologists administered a set of screening questionnaires: Mini Mental State Examination (MMSE), Geriatric Depression Scale – Short Form (GDS-SF), Functional Assessment Questionnaire, and Hachinski Ischemic Score. They then interviewed each participant and performed a thorough neuropsychological assessment. Based on this information, the evaluators placed each participant in a specific diagnostic group; participants were diagnosed with MCI using the criteria outlined by Petersen and Grundman [26]. Also, only those MCI patients who had memory impairment (aMCI) were included in the study.

The sample for the analyses only included participants aged 60 years or older. The exclusion criteria employed were the following: (1) history of psychiatric or neurological disorders, (2) evidence of infection, infarction or focal lesions in a T2-weighted scan within 2 months prior to the MEG acquisition, (3) consumption of drugs that could affect MEG recordings (e.g., cholinesterase inhibitors), (4) alcoholism, (5) chronic use of anxiolytics, narcotics, anticonvulsants or sedative hypnotics, and (6) a modified Hachinski score of 5 or more. Additional analyses were carried out to discard causes of aMCI other than dementia (diabetes mellitus, thyroid problems, vitamin B12 deficit, syphilis, and HIV). For the control group, participants with an MMSE score of less than 27 were excluded, as well as those who reported Subjective Memory Complaints in the clinical interview.

Table 1 Descriptive characteristics of the control and aMCI groups

Variable	Controls (mean ± SD) Women mean / Men mean	aMCI (mean ± SD) Women mean / Men mean
Sex (W)	105 (61%)	69 (66%)
Age (years)*	69.4 ± 5.3 69.4 / 69.3	74.0 ± 4.6 73.7 / 74.5
Education (years)*	14.6 ± 5.1 13.8 / 15.7*	8.5 ± 4.7 7.8 / 9.8
MMSE*	29.2 ± 1 29.2 / 29.0	26.4 ± 2.5 26.2 / 26.9
Inverse digits*	6.2 ± 2.1 5.8 / 6.8*	3.9 ± 1.4 3.8 / 4.28
BNT*	54.2 ± 6.2 53.3 / 55.7*	44.7 ± 10.5 44.1 / 46.0
TMT-B (seconds)*	105.0 ± 57.4 114.0 / 91.4*	234.0 ± 103.3 255.0 / 201.0*
LM-immediate*	39.3 ± 11.9 38.8 / 40.0	15.4 ± 7.9 14.6 / 16.9
LM-delayed*	23.8 ± 9.3 24.1 / 23.2	6.0 ± 5.9 5.4 / 7.0

*$P < .05$ (P (sex) > 0.05), indicated in the variable column for group differences and in each group column for sex differences in each group; Mann-Whitney non-parametric test or Pearson's test, as appropriate

aMCI amnestic Mild Cognitive Impairment, *MMSE* Mini Mental State Examination, *BNT* Boston Naming Test, *TMT-B* Trail Making Test B, *LM* Logical memory

MEG recordings

We recorded brain activity using a 306 channel Vectorview MEG system (Elekta AB, Stockholm, Sweden), which consisted of 102 magnetometers and 204 planar gradiometers. The MEG system was housed in a field-isolated room (VacuumSchmelze GmmbH, Hanau, Germany) at the Center for Biomedical Technology in Madrid, Spain.

Recordings were obtained under eyes-closed resting-state conditions and lasted 4 to 5 min, at a 1000 Hz sampling rate with an online anti-alias bandpass filter (cut-off frequency filtering of 0.1 to 330 Hz). We used a 3D Fastrak Polhemus digitizer to computerize the head shape, which captured around 300 points on the scalp surface and three anatomical reference points (nasion and left and right preauricular points). During the register, the device also recorded head position using four head position indication coils placed on the forehead

and mastoids. Eye movements and blinks were registered using two bipolar electrooculogram electrodes placed above and below the left eye and a ground electrode attached to the upper cheek.

Preprocessing

We preprocessed the electrophysiological data using the Fieldtrip toolbox version 20,170,501 [27] and in-house Matlab scripts (version 2021b). The pipeline included the following steps: (1) detecting and removing noisy channels using Maxfilter software, which virtually reconstructed their activity; (2) removing magnetic noise from outside the head and compensating for head movements using Temporal Signal Space Separation (tSSS) [28]; (3) removing SQUID jumps and muscular artifacts through ocular inspection; (4) removing the contribution of ocular and cardiac activity to the MEG signal through the use of the Second Order Blind Identification (SOBI) algorithm [29] based on Independent Component Analysis (ICA); (5) segmenting the continuous data into 4-second epochs with 2-second padding on each side to avoid edge effects.

Following data preprocessing, we used a source model to reconstruct the activities of distinct brain locations, referred to as sources. Our source model consisted of a regular grid of 4560 points spaced 1 cm apart forming a cube. 2459 of those were placed inside brain tissue, as specified the Montreal Neurological Institute (MNI) template. For all further analyses, we considered only the 1210 sources belonging to 80 cortical regions according to the first version of the Automated Anatomical Labelling (AAL) [30]; excluded regions were the amygdala, the caudate, the putamen, the pallidum and the thalamus.

We linearly transformed the structural information of the source model to the individual 3D image of the head obtained using the Fastrak Polhemus, adjusting the size of the inner skull surface. This allowed us to construct a single shell model, which we used to calculate the lead field matrix through a modified spherical solution [31].

MEG data were band-pass filtered between 2 and 45 Hz using a 450th-order finite input response (FIR) filter designed with a Hann window. To avoid phase distortion, a two-pass filtering approach was used. In addition, to mitigate edge effects, 2000 samples of real data padding were added to each side of the signal.

Finally, the activity of each participant on each source was reconstructed using a Linearly-Constrained-Minimum-Variance (LCMV) beamformer [32]. This is a widely used technique that spatially filters the MEG data to identify the activity of specific brain sources, while reducing interference from other sources.

Graph construction

A graph is a mathematical representation of a network of elements, called nodes, that are connected by links, known as edges. It is typically expressed as an ordered pair, $G = (V, E)$, where V is a set of nonempty nodes and E is a set of edges, each denoting a connection between two nodes. Additionally, edges can have values assigned to them, known as weights, which represent the distance between the nodes an edge connects.

In the context of brain networks, nodes correspond to brain regions, and edges correspond to some sort of connection between them. In this study, nodes correspond to cortical sources from the AAL in five frequency bands independently, and edges correspond to the functional connectivity values between them. Consequently, we ended up using graphs containing 6050 nodes (1210 cortical sources across five frequency bands) and weighted, undirected edges. Despite the added computational complexity, we chose to use sources instead of brain regions and to keep the weights instead of binarizing the graphs to avoid the significant loss of information that these would entail.

We calculated functional connectivity between all nodes using corrected amplitude envelope correlation (AEC) (Fig. 1). AEC has been frequently used to measure synchrony, both within a single frequency band and across different bands [33–35], and its corrected version accounts for potential biases in the correlation measure. Previous studies have shown that corrected AEC has higher reproducibility and reliability than phase- or coherence-based metrics in MEG [36, 37].

Functional connectivity calculation involved four steps: (1) dividing each source signal into five frequency bands (delta: 2–4 Hz, theta: 4–8 Hz, alpha: 8–12 Hz, beta: 12–30 Hz, and gamma: 30–45 Hz), (2) orthogonalizing each source time series to eliminate source leakage, (3) calculating the envelopes of each source activity in each frequency band using the Hilbert transformation [38], and (4) quantifying functional connectivity as the Pearson correlation coefficient between envelopes [39]. The absolute values of the coefficients were used as the weights of the edges in the graphs. We refrained from setting a cutoff value for these weights to prevent introducing biases in graph structure that arise from selecting a specific threshold.

As a result, the brain activity for each participant was represented as a single cross-frequency graph, in which each node was connected to every other node across all frequency bands. This approach allows us to consider both intra- and inter-band edges, as opposed to the more typically employed frequency-specific approaches that ignore inter-band interactions (Fig. 1B, lower part).

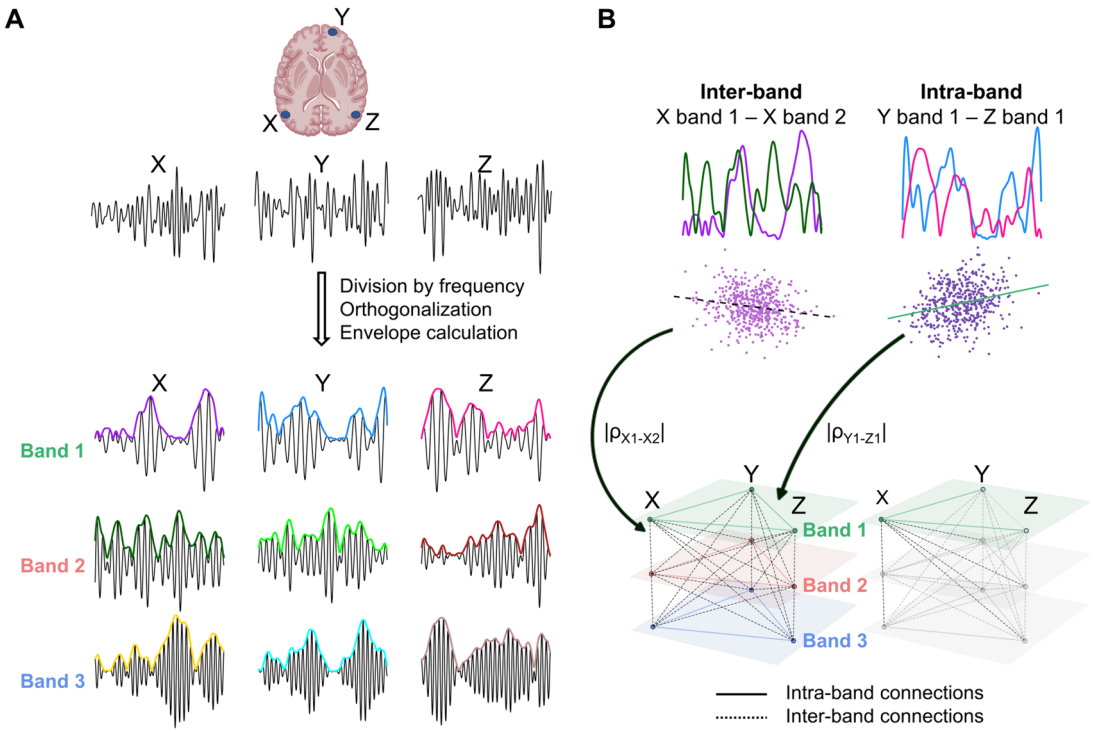

Fig. 1 Schema of cross-frequency graphs. For simplicity, we display only three brain sources (X, Y, Z) and three frequency bands (Band 1, Band 2, Band 3), although in the study 1210 brain sources and five frequency bands were used. (A): we calculated the MEG signal of each source, which was then divided by frequency; the signals were then orthogonalized, and the envelopes calculated. The absolute value of the Pearson correlation between envelopes was used as weight for the graph edges. (B): the upper panels show two examples of the correlation calculation: one for inter-band connections and one for intra-band connections; the lower panels display the resulting graph (left) and outline how each node has intra-band connections (solid-colored lines) and inter-band connections (dotted-black lines), accounting for the interplays between bands (right). Although they are represented differently in the figure, both types of edges were treated equally in the centrality metrics' calculations

Centrality calculation

We used three graph measures as centrality indicators: node strength, eigenvector centrality, and betweenness centrality. All these measures were calculated for each node of each subject using the NetworkX library (version 2.6.3) and the SciPy library (version 1.7.1) in Python (version 3.10.4).

The strength of a node quantifies the node's direct connections to other nodes in the graph. It is calculated as the sum of the weights of the links incident to node i:

$$s_i = \sum_{j \neq i} w_{ij},$$

where w_{ij} is the weight of the link between nodes i and j.

The eigenvector centrality of a node estimates the relevance of the nodes to which it is directly connected. It is calculated from the following equation:

$$Mv = \lambda v,$$

where M is the adjacency matrix, λ the eigenvalues and v the eigenvectors. The element i of the eigenvector v that is associated with the largest eigenvalue λ_1 holds the value for the eigenvector centrality of node i.

Finally, the betweenness centrality of a node measures the extent to which the node lies on the shortest paths between other nodes. The shortest path between two nodes is the path with the minimum sum of weights. The betweenness centrality of a node i is calculated as the sum of the fraction of the number of shortest paths between all node pairs that pass through node i:

$$B_i = \sum_{j,\ k \in V} \frac{\sigma(j,k|i)}{\sigma(j,k)},$$

where V is the set of nodes, $\sigma(j,k)$ is the number of shortest paths, and $\sigma(j,k|i)$ is the number of those paths passing through some node i other than j, k. As betweenness centrality takes link weights as a distance measure, we used the inverse of the weights (which, in our case, indicate functional proximity).

To reduce computation time, betweenness centrality was estimated using the algorithm developed by Brandes and Pich [40]. This algorithm allows for the efficient

estimation of betweenness centrality by considering only a specified number of random nodes (k). In this study, the value of k was set to 250, which provided stable estimates.

This resulted in three vectors per subject, each with a length of 6050 (composed of five blocks, each containing 1210 values that correspond to the sources in each frequency band). To obtain a comprehensive measure of centrality, we combined the three metrics into one, hereafter referred to as centrality score. To account for the different numeric ranges of the metrics, we first z-scored each of the three vectors independently and then averaged them to obtain a fourth vector of the same length for each subject, the centrality score.

In addition to calculating the centrality score at the frequency band level, we also calculated its band average. To do so, we divided the centrality score vector into its five blocks, each corresponding to a frequency. We then z-scored each block independently, to ensure equal contributions from all bands, and averaged the five scaled blocks, obtaining a single vector of length 1210.

Statistical analysis of centrality metrics

The four centrality measures were compared between the control and aMCI groups using Matlab (version 2021b). A three-way factorial ANOVA was conducted, with age and years of education as covariables and an alpha level of 0.05. The ANOVA analysis was non-parameterized by using permutations; each F-value obtained for the real data was compared with the F-values obtained for 10.000 randomizations of the original group assignment, which enabled us to calculate the permutation-corrected p-value for each F-value.

To account for the large number of comparisons conducted, we employed the two-sided cluster-based permutation test (CBPT), using a Montecarlo approach [41]. Significant sources were grouped in clusters according to their spatial proximity (alpha level of 0.05). Cluster-level statistics were calculated by summing the F-values of all sources within each cluster and comparing that F-value to the null distribution of cluster size, which was obtained through 10.000 randomizations of the group assignments. Only significant clusters after multiple comparisons correction are reported in the results section.

Contribution of intra- and inter-frequency couplings

To investigate the role of cross-frequency couplings in our analysis, we studied the isolated contribution of each pair of frequency bands, both intra- and inter-band, considering only the sources that were significant in between-group comparisons for each centrality metric.

As a starting point, we used each participant's original graph, with 6050 nodes (1210 sources x 5 frequency bands). We extracted subgraphs for each type of interaction: intra-band interactions (e.g., delta-delta, theta-theta) and isolated inter-band interactions (e.g., delta-theta, delta-alpha). These subgraphs represent the relationships either between a single band or between different pairs of bands.

Then, we calculated the three centrality metrics (strength, eigenvector centrality, and betweenness centrality) for each subgraph, considering only the edges that involve at least one node identified as significant for each centrality metric. For instance, to evaluate the specific influence of the delta-alpha interactions on the significant delta cluster in eigenvector centrality, we focused on the delta-alpha subgraph and excluded links not involving nodes from the delta significant cluster.

After computing the centrality metrics for all subgraphs across subjects, we calculated the centrality score as described in the main text. Then, we averaged the calculated values for significant sources within each centrality score cluster. This resulted in a mean centrality score for each band's significant cluster across all interactions, yielding 25 values per subject. Finally, we performed an ANOVA for each interaction (25 in total) with age and years of education as covariates.

We then used stepwise logistic regression, which is a method of model selection that chooses the most important predictor variables by adding or removing predictors based on their statistical significance. We designed a stepwise logistic regression model for each frequency band, trying to predict the group (aMCI or control) using the mean centrality values extracted from the isolated interactions between two specific bands.

Results

In this study, we compared strength, eigenvector centrality, and betweenness centrality in each brain source and frequency band between aMCI and control participants (Fig. 2). It is important to bear in mind that our analyses incorporated cross-frequency interplays to reflect the interactions between oscillatory activity in each source within a given band and all other sources across all bands.

Strength

Our results indicate that node strength decreased in the aMCI group in various frequency ranges, particularly in posterior and temporal brain regions (Fig. 2A). In the alpha band, areas with a lowered strength included regions posterior to the precentral gyrus (lateral and medial aspects of the parietal and occipital lobes) and the temporal lobe ($F_{sum} = 3291$, $p_{cluster} = 0.0276$). The beta band cluster of decreased strength comprised these same areas and included motor regions and the anterior cingulate cortex bilaterally ($F_{sum} = 8112$, $p_{cluster} = 0.0054$).

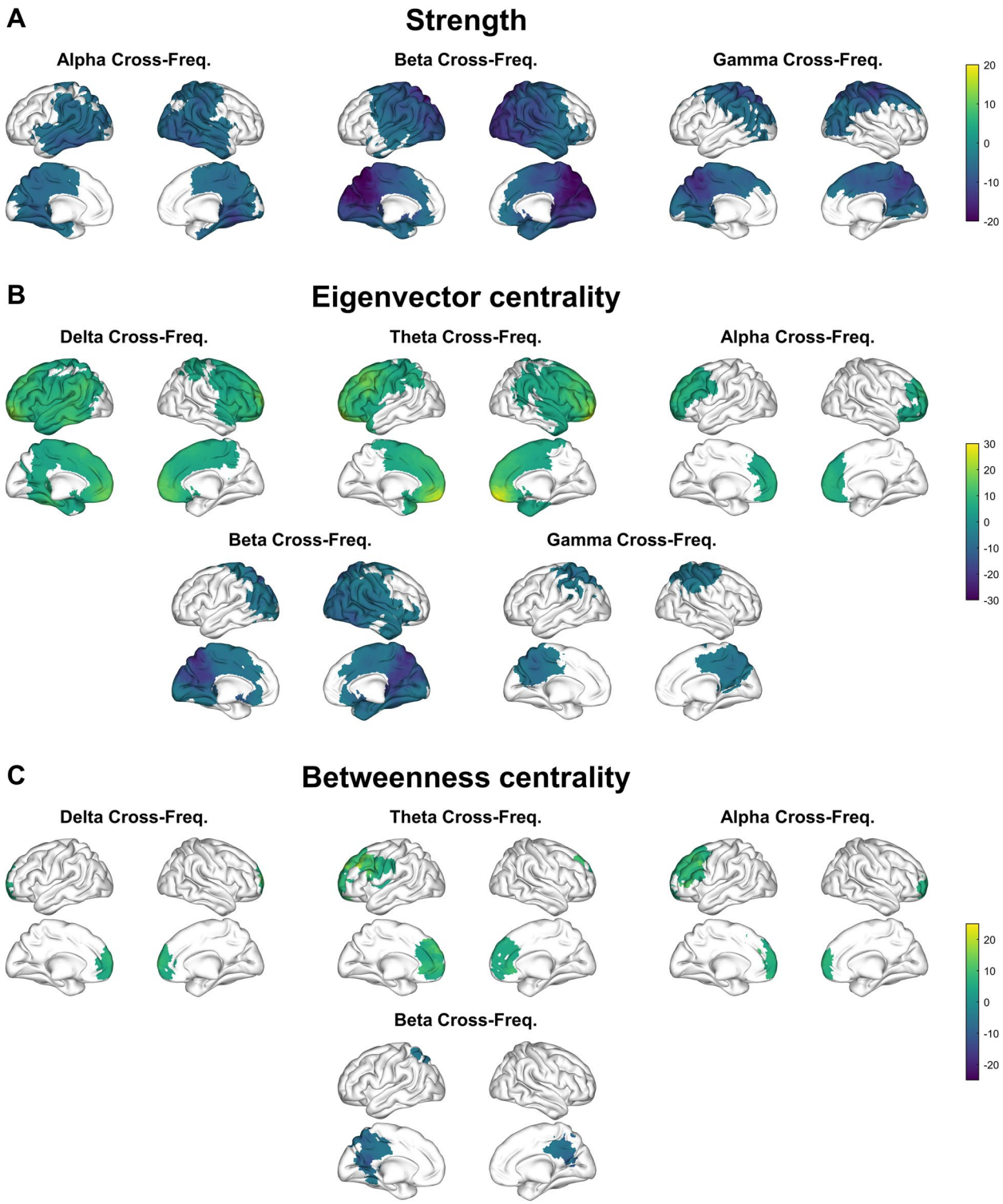

Fig. 2 Centrality disruption in MCI assessed with strength (A), eigenvector centrality (B), and betweenness centrality (C). The colored regions indicate significative differences between the aMCI and control groups, and the color scale represents the F-value of each source: positive values (greenish colors) denote significant sources with increased centrality in aMCIs, while negative values (blueish colors) represent significant sources with decreased centrality in aMCIs. For each measure, only bands with at least one significant cluster are shown. The centrality metric of each band includes the links of nodes in that band with the nodes in that same and other bands

Finally, the gamma band showed a decrease in strength in a smaller portion of the cortex, including the posterior, occipital and posterior part of the frontal lobe ($F_{sum} = 3856$, $p_{cluster} = 0.0158$). Notably, all posterior areas of the default mode network were affected, including the hippocampus and parahippocampus bilaterally in alpha and beta, and the precuneus and cingulate gyrus bilaterally in all three bands.

Eigenvector centrality

Eigenvector centrality showed a combined pattern of centrality disruption in the aMCI group. It increased mainly in the anterior regions in the delta, theta, and alpha bands and decreased in the temporal and posterior areas in the beta and gamma bands (Fig. 2B). In the delta band, the centrality increase affected the frontal and parietal lobes, as well as the left temporal lobe ($F_{sum} = 5776$, $p_{cluster} = 0.0032$). We found a similar cluster in the theta band, including the same regions except the temporal lobe ($F_{sum} = 5545$, $p_{cluster} = 0.0009$). In contrast, in the alpha band, we only found an increase in eigenvector centrality in the frontal lobe ($F_{sum} = 1122$, $p_{cluster} = 0.0064$). Concerning decreases in eigenvector centrality, the beta band showed changes in the parietal lobe (extending more anteriorly over the lateral surface of the right hemisphere, including the temporal lobe) and the occipital lobe bilaterally ($F_{sum} = 4819$, $p_{cluster} = 0.0020$). Finally, the eigenvector centrality of gamma band showed alterations in a smaller cluster, affecting the precuneus and superior parietal cortex bilaterally ($F_{sum} = 1235$, $p_{cluster} = 0.0304$). Once again, the areas of the default mode network were affected: eigenvector centrality increases occurred in the prefrontal and anterior cingulate cortices, while decreases affected the middle and posterior cingulate cortex, precuneus, parahippocampus and right hippocampus.

Betweenness centrality

Finally, betweenness centrality showed a similar dual pattern of increases and decreases in the aMCI group, although the clusters were remarkably smaller than in previous metrics. We found a betweenness increase affecting the prefrontal lobe in delta ($F_{sum} = 151$, $p_{cluster} = 0.0102$), theta ($F_{sum} = 594$, $p_{cluster} = 0.0002$), and alpha (two significant clusters were found: $F^1_{sum} = 265$, $p^1_{cluster} = 0.0006$; $F^2_{sum} = 130$, $p^2_{cluster} = 0.0064$), and a decrease over posterior areas of the brain (including the cingulate gyrus and the precuneus bilaterally) in beta ($F_{sum} = 208$, $p_{cluster} = 0.0002$).

Centrality score

We integrated the results of the three classical measures into a single measure, the centrality score, ensuring an equal contribution of all bands and metrics. The results include changes in centrality for each band and for the band average (Fig. 3).

Analysis of individual bands revealed that the aMCI group exhibited an increase in centrality in the delta ($F_{sum} = 1759$, $p_{cluster} = 0.0346$) and theta ($F_{sum} = 2118$, $p_{cluster} = 0.0126$) bands over frontal areas, whereas we observed a decrease in centrality in posterior brain regions across the alpha ($F_{sum} = 815$, $p_{cluster} = 0.0436$), beta ($F_{sum} = 5542$, $p_{cluster} = 0.0004$), and gamma ($F_{sum} = 2238$, $p_{cluster} = 0.0092$) bands. Specifically, centrality reductions affected the parietal lobe in all three bands, the temporal lobe in alpha and beta, and the occipital lobe in beta.

When considering the band average, we observed a combination of the previously observed dual pattern of centrality disruption, with increased centrality affecting the frontal lobe ($F_{sum} = 797$, $p_{cluster} = 0.0284$) and decreased centrality affecting temporo-parietal areas ($F_{sum} = 1699$, $p_{cluster} = 0.0090$). Remarkably, all the areas of the default mode network were implicated in these results.

Figure 3 also shows the contribution to the significant clusters of each specific interaction between frequency bands. In delta, the interactions between bands that discriminate significantly between the two groups are delta-alpha ($F = 6.57$, $p = 0.0109$), delta-beta ($F = 5.48$, $p = 0.0200$), and delta-gamma ($F = 6.67$, $p = 0.0103$); in theta, all interactions are significant: theta-delta ($F = 10.43$, $p = 0.0014$), theta-theta ($F = 12.13$, $p = 0.0006$), theta-alpha ($F = 14.09$, $p = 0.0002$), theta-beta ($F = 7.61$, $p = 0.0062$), and theta-gamma ($F = 10.01$, $p = 0.0017$); in alpha, significant interactions include alpha-theta ($F = 4.16$, $p = 0.0424$), alpha-alpha ($F = 15.46$, $p = 0.0001$), alpha-beta ($F = 12.29$, $p = 0.0005$), and alpha-gamma ($F = 7.28$, $p = 0.0074$); similarly, beta significant interactions are beta-theta ($F = 3.95$, $p = 0.0478$), beta-alpha ($F = 11.50$, $p = 0.0008$), beta-beta ($F = 21.01$, $p < 0.0001$), and beta-gamma ($F = 113.02$, $p = 0.0004$); finally, all of gamma interactions are significant: gamma-delta ($F = 8.33$, $p = 0.0042$), gamma-theta ($F = 9.67$, $p = 0.0021$), gamma-alpha ($F = 13.57$, $p = 0.0002$), gamma-beta ($F = 18.03$, $p < 0.0001$), and gamma-gamma ($F = 14.89$, $p = 0.0001$).

As a final test for the contribution of pairwise interactions between bands to each cluster, we built a stepwise logistic regression model for each frequency band, using the mean centrality values of pairwise interactions as predictors and the group as criterion. All models turned out significant ($p < 0.005$), and the included predictors were: for delta cluster, centrality from delta-beta interactions; for theta, centrality from theta-delta and theta-alpha; for alpha, centrality from alpha-beta; for beta, centrality from beta-alpha, beta-beta and beta-gamma; and for gamma, centrality from gamma-beta.

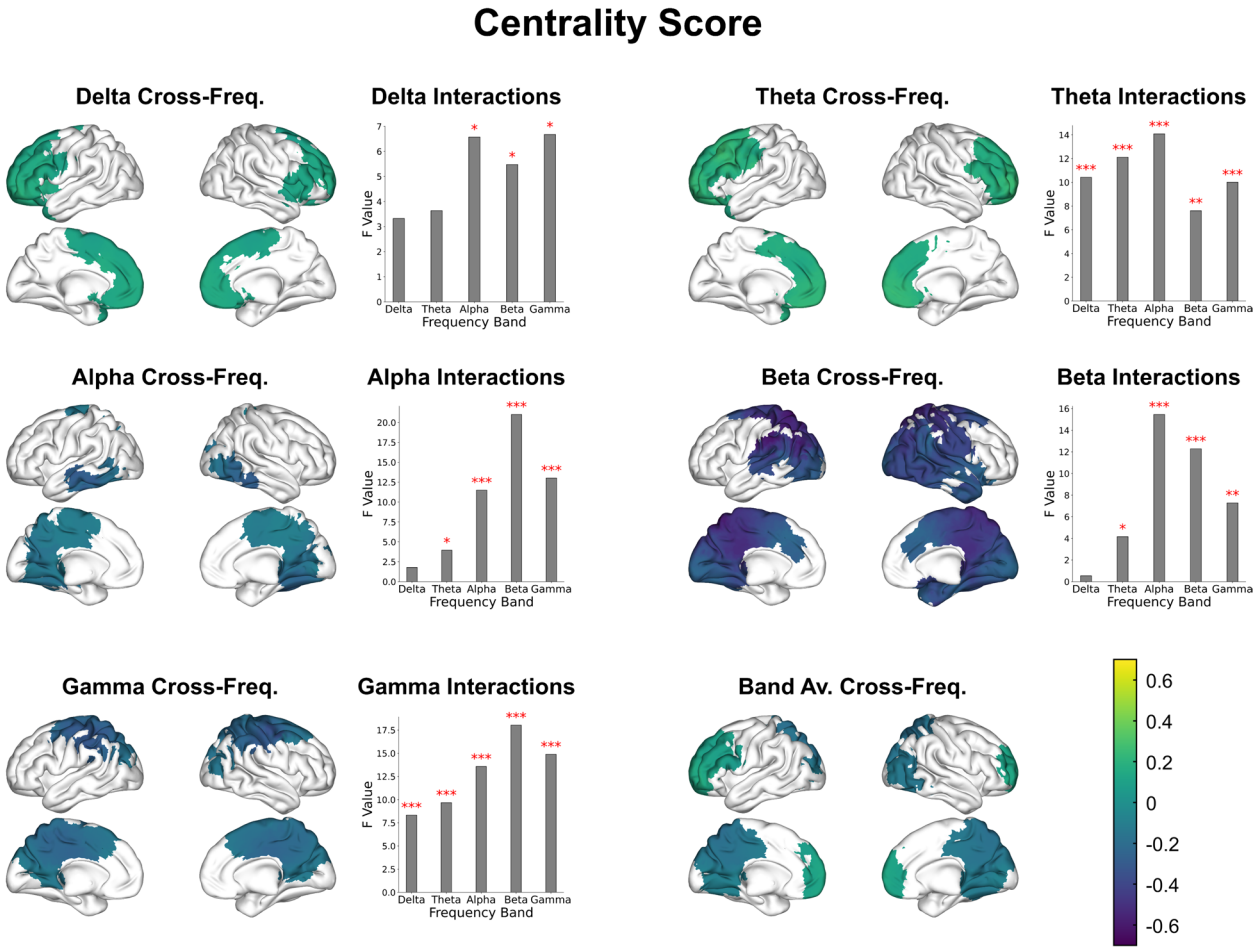

Fig. 3 Centrality disruption in aMCI assessed with the centrality score. The color code is the same as in Fig. 2. For each of the five classical frequency bands, an additional graph is displayed, showing the isolated contribution of each par of frequency bands to the significant cluster of that band. The x-axis shows the interaction band, while the y-axis shows the F-value of an ANOVA that discriminates both groups (controls and aMCIs) with age and years of education as covariables

Discussion

This study shows that changes in brain communication patterns in aMCI impact the overall structure of brain networks in two distinct ways: posterior areas reduce their relative importance by decreasing the synchrony between their own high-frequency oscillations and the activity of other regions in all frequency bands, whereas anterior regions increase their importance by synchronizing their low-frequency oscillations with the activity of other regions in all frequencies. Notably, this is the first MEG study to examine network impairment in aMCI using a multilayer, source-based framework, and our findings demonstrate that the changes in functional connectivity typically observed in aMCI entail a disruption in the global functional network structure. Furthermore, we have demonstrated that cross-frequency interactions contain relevant information in the analysis of centrality changes in aMCI.

Electrophysiological studies investigating information flow in the brain typically use a simplified framework, limiting communication analysis to brain regions oscillating within the same frequency bands [22]. However, previous literature has revealed robust interactions between brain regions with different oscillatory rhythms; for example, theta-gamma coupling plays a major role in both working memory [42] and long-term spatial memory [43]. In this sense, our work extends the current understanding of changes in information flow in the early stages of AD by emphasizing the impact of the observed alterations on both intra- and inter-band communication between sources.

Remarkably, and in contrast to most of the previous literature [22], we constructed source-based graphs that were completely connected and weighted. Despite the technical challenges associated with these large-scale graphs, this holistic approach allowed us to capture the

intricate network structure without oversimplification. On these graphs, we assessed centrality changes in aMCI. In the context of brain networks, exploring a variety of centrality measures can provide deeper insights on inter-regional interactions [44]; thus, to better understand how information flow changes in the quite complex patterns of brain communication, we created an integrative centrality score. This centrality score combines three of the metrics most employed in isolation to address this matter [45], merging the complementary aspects of centrality in the results of our centrality score.

Our analyses comparing the centrality scores between aMCI and control participants reveal two distinct patterns: a spatial pattern and a frequency pattern. The spatial pattern shows that posterior areas reduce their relative contribution to network communication in favor of anterior regions, that show increases in centrality. The frequency pattern shows that the aMCI group has decreased centrality through fast-frequency communication and increased centrality through slow-frequency communication.

The result for the band average cross-frequency coupling in the global centrality score metric depicts the above-mentioned spatial pattern, with the aMCI group showing a centrality decrease over posterior regions and an increase in anterior areas. This underscores that certain brain regions' centrality is significantly and consistently compromised in the early course of the disease, regardless of the specific metric or frequency range. These findings align with existing observations on functional connectivity disruptions in aMCI due to AD, that report hypoconnectivity in posterior areas and hyperconnectivity in anterior regions [12, 13, 46, 47]. This posterior-to-anterior shift has been previously reported in the PASA model [48] and other studies [49]. Furthermore, the centrality changes we report affect all the main areas of the default mode network (including medial prefrontal cortex, cingulate cortex, precuneus, and angular gyrus), which is consistent with previous studies showing that these brain regions are particularly vulnerable to AD pathology [50–52], and might be related to memory impairment [53]. Furthermore, the medial temporal lobe (MTL) system, also associated with memory disruption in AD and MCI in the literature [53, 54], is shown to be affected in our study. Another network in which functional connectivity disturbances are typically found in AD, and which we have found to have centrality disruption, is the frontoparietal network: the dorsolateral, anterior, and ventral lateral prefrontal cortices show centrality increases, while the posterior parietal cortex and inferior parietal lobule exhibit centrality decreases. However, our results broaden previous evidence suggesting that alterations in functional connectivity translate into changes in the way information propagates through the brain, affecting the overall relevance of extensive brain regions to network communication, as measured by centrality.

The decline in centrality in aMCI over posterior areas observed in our results is highly consistent with AD, which entails a disconnection condition [55]. The abnormal expression of tau primarily contributes to this phenomenon [12], as it affects the cytoskeleton of neurons and leads to synaptic loss [12, 55]. Other studies link hypometabolism with reduced functional connectivity [15], further supporting these findings.

While disconnection signs have been unanimously interpreted as a pathological sign by previous literature, the biological implications of the network centrality increase we observe in the aMCI group over anterior brain areas is subject to more debate. Traditionally, neuroscientists have suggested that functional connectivity increases may palliate some of the burden produced by decreased connectivity in posterior areas of the brain, acting as a compensatory mechanism [56]; one example is the PASA model [48], in which shift in brain activations is seen as an offsetting process. However, this increased activity entails the accumulation of residuals, which eventually can lead to more significant cognitive declines [57]. Recent research provides an alternative pathological explanation for this phenomenon [58]. This hypothesis proposes that Aβ plaques affect preferentially inhibitory neurons, which leads to an increase in excitability, which could result in functional connectivity upregulations. Several studies reinforce this idea by demonstrating that pyramidal neurons in contact with plaques lose GABAergic synapsis [59], that Aβ causes neuronal hyperactivity [60], and that Aβ colocalizes with hypersynchrony, but not with hyposynchrony [12].

According to this framework, the centrality increase would be interpreted as a pathological sign, contributing to the cascading network failure by increasing neural noise and leading to neuronal death through heightened excitotoxicity. Numerous studies support this theory by showing a widespread loss of functional connectivity among advanced AD patients, including frontal regions [61–63]. Furthermore, Damoiseaux et al. (2012) performed a longitudinal study in which they measured the functional connectivity of AD patients twice (two to four years apart) using fMRI: the first scan revealed connectivity increases in anterior areas of the default mode network and connectivity decreases in posterior areas, while the second scan showed connectivity decreases in all areas. These findings reinforce hyperexcitability as a precursor to hypoexcitability. Nonetheless, we must state that we carried out correlation analyses, not shown in this article, which did not reveal any significant relationships between the connectivity increases in frontal regions and

cognitive performance for the aMCI group; for this reason, using our available data, we cannot support either the compensatory or the pathological hypothesis.

On the other side, the frequency pattern displays centrality increases in low-frequency bands (delta and theta) and centrality decreases in high-frequency bands (alpha, beta, and gamma). It is important to note that the centrality changes we have presented involve the interactions of nodes of one frequency band with each other and with nodes of other bands, as explained in the previous sections. These results suggest that certain brain regions (more concretely anterior areas) increase their relevance in the network by increasing the coupling of its own slow wave activity with other parts of the network, regardless of the latter´s frequency range. Nonetheless, our results are congruent with previous findings on functional connectivity in aMCI and AD, that link increments in synchrony mainly to delta and theta and decrements to alpha and beta activity [10–12, 14, 15]. In addition, some studies report hyperconnectivity in the alpha range over anterior regions [13], whereas hypoconnectivity has rarely been associated with gamma [16].

Interpreting the specific meaning of the frequency pattern emerging from our results is challenging due to the limited understanding of the human resting state dynamics and the role different frequency bands play in AD. Previous studies have found an increase in power for the delta and theta bands, as well as a decrease for the alpha and beta bands [47, 64, 65]. This pattern may relate to a loss of synapses, which can impede communication between brain regions, as information can flow through fewer "pathways". In this regard, Cabral et al. [66] used a computational model to demonstrate how reductions in coupling strength can lead to increased slow-frequency activity. In line with this hypothesis, several studies have reported decreased activity of both theta [62] and even delta [63] during later stages of the disease progression. In this vein, our results could reflect an intermediate state in which some regions exhibit a diminished ability to contribute to network communication while oscillating in faster rhythms, whereas others show an increased relevance in slower frequencies, resembling the pattern of alterations suggested by the mentioned studies.

When analyzing each individual metric, we observe that both the spatial and frequency patterns are apparent. This was expected, as the three metrics represent centrality. Nevertheless, it is worth noting that the metrics reflect different aspects of a node's significance: node strength measures the number and intensity of connections a node has, eigenvector centrality considers the relevance of said connections, and betweenness centrality estimates the capacity of a node to connect other nodes in the network through shortest paths.

As a result of these nuances, each metric yields unique results. The results for node strength only show decreases in alpha, beta, and gamma bands. Remarkably, most of the brain is affected, even the posterior parts of the frontal lobe. This might be due to the neuronal death that AD entails. Remarkably, no increases in strength were observed, meaning that none of the regions exhibit a significant increase in the magnitude of its raw total connection to the rest of the network.

The results for eigenvector and betweenness centrality show increases in delta, theta, and alpha, alongside decreases in beta (both metrics) and gamma (only eigenvector centrality). These findings reinforce the loss of coordination in the posterior brain regions, but also highlight heightened centralization within the frontal cortex. This might be due to the disconnection occurring among posterior areas, which appears responsible for shifting relative importance towards anterior brain regions—a phenomenon previously reported [64, 67].

Another noteworthy feature is the variable centrality changes displayed by the alpha band, depending on the metric. This finding might suggest a transitional frequency role between faster and slower brain rhythms for the alpha band in the maintenance of the global communication structure. While the role of the beta and theta activity is consistently altered towards decreased and increased centrality respectively, alpha band activity seems to display both patterns depending on the aspect of centrality we pay attention to.

Lastly, it is remarkable that betweenness centrality alterations in the aMCI group affect a smaller portion of the network than changes in the other metrics. This is likely due to betweenness centrality being a more global measure that considers all other nodes in the network—reflecting higher-scale aspects of centrality—while strength and eigenvector centrality are more local, depending mainly on a node's immediate neighbors. Thus, the smaller disruption in betweenness centrality may indicate that while local changes are pronounced, the overall information flow structure of the network is less affected. This observation underscores the importance of considering different centrality measures to gain a comprehensive understanding of global network dynamics.

Furthermore, future research exploring global graph metrics, such as small-worldness and modularity, could provide further insights in the broader impacts of the disease on network efficiency and modular organization. Applying these metrics in the context of multilayer networks could reveal new aspects of brain connectivity

that are not captured by local centrality measures alone. It should be noted that, in this work, corrected AEC was selected to calculate functional connectivity. Previous studies have shown that different functional connectivity measures reflect distinct neural mechanisms, at least to a certain degree [68]. Therefore, the election of an amplitude-based metric, instead of a phase- or amplitude-phase-based metric, must be considered when comparing our results with other works employing other connectivity metrics.

One last remarkable finding of this study is the important contributions of cross-frequency couplings to the study of functional disruptions. Our results show that interactions between different frequency bands are highly discriminative between groups. We find a pattern where, while the faster bands (alpha, beta, and gamma) influence themselves and the slower bands, the slower bands seem to have less influence on themselves and others. Both alpha and beta, which are the frequency bands more strongly associated to AD—being posterior decreases in these bands the most common finding in MCI and AD research [69]—influence all other bands and themselves. Similarly, gamma band also influences all five frequency bands, which again is not surprising as recently many articles have stated its importance in AD [70]. On the other side, delta and theta bands have the lowest influence on the faster bands (alpha, beta, and gamma), and also in delta. An explanation for this could be the aforementioned phenomenon where, at a loss of synapses, there is a decrease in fast oscillations which in turn increases the activity in slow oscillations—i.e., a loss of alpha, beta and gamma activity due to the loss of direct communications between neurons would lead to an increase in the slower communications. Under this line of thought, while now we see that delta is the least influenced by other bands, we could expect it to be more affected in later stages of the disease. However, further work is required to test these hypotheses. Lastly, it is noteworthy that the theta and gamma bands are the ones influenced by all the other bands; in both it has been shown that their cross-frequency couplings are relevant in different cognitive processes [42, 43]. In any case, cross-frequency couplings should be considered in posterior studies in this matter, as they provide a valuable source of information.

Limitations

The main limitation of this study is the lack of biomarkers, leading to some uncertainty about the presence of AD in all subjects with aMCI. However, it is worth noting that all patients exhibited memory impairment, which is strongly linked to the subsequent development of AD in particular [71, 72]. However, future studies should include biomarker data to better characterize the relationship between centrality changes and disease progression in AD. Another limitation that must be considered is the lack of individual T1 data, reason why in this study we used a standard template. Finally, it must be noted that no empty room recording was performed to assess sensor noise, and instead recorded data underwent visual and automatic inspection to guarantee a good signal-to-noise ratio; furthermore, we applied the MaxFilter tSSS to all recordings to minimize sensor noise.

Conclusions

Overall, our findings shed light on the complex changes that occur in brain networks in the early stages of AD. The results indicate a noteworthy shift in centrality distribution from posterior to anterior regions, indicating a decline in relative significance of the former and an increase in importance of the latter. These findings demonstrate a remarkable level of consistency, with congruent outcomes across all bands and metrics, suggesting that using a unified approach that considers the interactions between different frequency bands can enhance our understanding of AD network dynamics in a more comprehensive manner. Furthermore, this study establishes a new approach to comprehensively study disruptions in cross-frequency functional networks not only for AD, but also for other neurological disorders studied through electrophysiology techniques.

Abbreviations

AEC	Amplitude envelope correlation
AD	Alzheimer's disease
aMCI	Amnestic Mild Cognitive Impairment
Aβ	Amyloid-β
AAL	Automated Anatomical Labelling
CBPT	Cluster based permutation test
MCI	Mild Cognitive Impairment
MMSE	Mini Mental State Examination
MNI	Montreal Neurological Institute

Acknowledgements

Not applicable.

Authors' contributions

FM and DLS conceived the study. SD and DLS obtained and preprocessed the electrophysiological recordings. IT generated all results from data. IT and DLS wrote a first version of the paper, and all authors contributed to the final version.

Funding

This study was supported by EU Horizon 2022 framework program funding to 'eBRAIN-Health' project (https://www.ebrains.eu/) to Ignacio Taguas.
The project that gave rise to these results received the support of a fellowship from the "la Caixa" Foundation (ID 100010434). The fellowship code is LCF/BQ/DR23/12000025. This work was funded by the Spanish Ministry of Science, Grant Ref. PID2021-122979OB-C21.

Availability of data and materials

The datasets used and/or analyzed during the current study are available from the corresponding author on reasonable request.

Declarations

Ethics approval and consent to participate

Informed consent was obtained from all participants. The ethics committee of Hospital Clínico San Carlos approved the study, and the procedure was carried out in accordance with the approved guidelines and regulations.

Consent for publication

Not applicable.

Competing interests

The authors declare no competing interests.

Author details

[1]Center for Cognitive and Computational Neuroscience, Complutense University of Madrid, Madrid 28015, Spain. [2]Department of Legal Medicine, Psychiatry and Pathology, Complutense University of Madrid, Madrid 28040, Spain. [3]Department of Experimental Psychology, Cognitive Psychology and Speech and Language Therapy, Complutense University of Madrid, Pozuelo de Alarcón 28223, Spain. [4]Health Research Institute of the Hospital Clínico San Carlos (IdISSC), Madrid 28240, Spain.

Received: 6 May 2024 Accepted: 13 September 2024
Published online: 09 October 2024

References

1. Duong S, Patel T, Chang F. Dementia: What pharmacists need to know. Can Pharm J (Ott). 2017;150(2):118–29.
2. Silva MVF, Loures CDMG, Alves LCV, De Souza LC, Borges KBG, Carvalho MDG. Alzheimer's disease: Risk factors and potentially protective measures. J Biomed Sci. 2019;26(1):33. https://doi.org/10.1186/s12929-019-0524-y.
3. Khanahmadi M, Farhud DD, Malmir M. Genetic of Alzheimer's Disease: A Narrative Review Article [Internet]. Vol. 44, Iran J Public Health. 2015. http://ijph.tums.ac.ir
4. Petersen RC, Parisi JE, Dickson DW, Johnson KA, Knopman DS, Boeve BF et al. Neuropathologic features of amnestic mild cognitive impairment. Arch Neurol. 2006;63(5).
5. Cheng YW, Chen TF, Chiu MJ. From mild cognitive impairment to subjective cognitive decline: Conceptual and methodological evolution. Vol. 13, Neuropsychiatric Disease and Treatment. 2017.
6. Fernández A, Hornero R, Mayo A, Poza J, Gil-Gregorio P, Ortiz T. MEG spectral profile in Alzheimer's disease and mild cognitive impairment. Clin Neurophysiol. 2006;117(2):306–14.
7. López M E, Cuesta P, Garcés P, Castellanos P N, Aurtenetxe S, Bajo R, et al. MEG spectral analysis in subtypes of mild cognitive impairment. Age (Dordr). 2014;36(3):9624.
8. Sun J, Wang B, Niu Y, Tan Y, Fan C, Zhang N et al. Complexity analysis of EEG, MEG, and fMRI in mild cognitive impairment and Alzheimer's disease: A review. Vol. 22, Entropy. 2020.
9. Friston KJ. Functional and effective connectivity: a review. Brain Connect. 2011;1(1):13–36.
10. Briels CT, Briels CT, Schoonhoven DN, Schoonhoven DN, Stam CJ, De Waal H, et al. Reproducibility of EEG functional connectivity in Alzheimer's disease. Alzheimers Res Ther. 2020;12(1).
11. Ruiz-Gómez SJ, Hornero R, Poza J, Maturana-Candelas A, Pinto N, Gómez C. Computational modeling of the effects of EEG volume conduction on functional connectivity metrics. Application to Alzheimer's disease continuum. J Neural Eng. 2019;16(6).
12. Ranasinghe KG, Cha J, Iaccarino L, Hinkley LB, Beagle AJ, Pham J, et al. Neurophysiological signatures in Alzheimer's disease are distinctly associated with TAU, amyloid-β accumulation, and cognitive decline. Sci Transl Med. 2020;12(534).
13. López-Sanz D, Bruña R, Garcés P, Martín-Buro MC, Walter S, Delgado ML et al. Functional connectivity disruption in subjective cognitive decline and mild cognitive impairment: A common pattern of alterations. Front Aging Neurosci. 2017;9(APR).
14. Núnez P, Poza J, Gómez C, Rodríguez-González V, Hillebrand A, Tola-Arribas MA et al. Characterizing the fluctuations of dynamic resting-state electrophysiological functional connectivity: Reduced neuronal coupling variability in mild cognitive impairment and dementia due to Alzheimer's disease. J Neural Eng. 2019;16(5).
15. Smailovic U, Koenig T, Savitcheva I, Chiotis K, Nordberg A, Blennow K, et al. Regional disconnection in alzheimer dementia and amyloid-positive mild cognitive impairment: association between eeg functional connectivity and brain glucose metabolism. Brain Connect. 2020;10(10):555–65.
16. Cuesta P, Ochoa-Urrea M, Funke M, Hasan O, Zhu P, Marcos A, et al. Gamma band functional connectivity reduction in patients with amnestic mild cognitive impairment and epileptiform activity. Brain Commun. 2022;4(2).
17. Nakamura A, Cuesta P, Kato T, Arahata Y, Iwata K, Yamagishi M, et al. Early functional network alterations in asymptomatic elders at risk for Alzheimer's disease. Sci Rep. 2017;7(1).
18. Farahani FV, Karwowski W, Lighthall NR. Application of graph theory for identifying connectivity patterns in human brain networks: a systematic review. 13, Frontiers in Neuroscience. 2019.
19. Fornito A, Zalesky A, Bullmore ET. Fundamentals of Brain Network Analysis. Fundamentals of Brain Network Analysis. 2016.
20. van den Heuvel MP, Scholtens LH, de Reus MA. Topological organization of connectivity strength in the rat connectome. Brain Struct Funct. 2016;221(3).
21. Kucikova L, Goerdten J, Dounavi ME, Mak E, Su L, Waldman AD, et al. Resting-state brain connectivity in healthy young and middle-aged adults at risk of progressive Alzheimer's disease, vol. 129. Elsevier Ltd; 2021. p. 142–53.
22. Miraglia F, Vecchio F, Pappalettera C, Nucci L, Cotelli M, Judica E et al. Brain Connectivity and Graph Theory Analysis in Alzheimer's and Parkinson's Disease: The Contribution of Electrophysiological Techniques. Vol. 12, Brain Sciences. 2022.
23. Binnewijzend MAA, Adriaanse SM, Van der Flier WM, Teunissen CE, de Munck JC, Stam CJ, et al. Brain network alterations in Alzheimer's disease measured by Eigenvector centrality in fMRI are related to cognition and CSF biomarkers. Hum Brain Mapp. 2014;35(5).
24. Yu M, Engels MMA, Hillebrand A, Van Straaten ECW, Gouw AA, Teunissen C, et al. Selective impairment of hippocampus and posterior hub areas in Alzheimer's disease: an MEG-based multiplex network study. Brain. 2017;140(5):1466–85.
25. De Domenico M, Sasai S, Arenas A. Mapping multiplex hubs in human functional brain networks. 2016.
26. Grundman M, Petersen RC, Ferris SH, Thomas RG, Aisen PS, Bennett DA et al. Mild Cognitive Impairment Can Be Distinguished From Alzheimer Disease and Normal Aging for Clinical Trials [Internet]. 2004. http://archneur.jamanetwork.com/
27. Oostenveld R, Fries P, Maris E, Schoffelen JM, FieldTrip. Open source software for advanced analysis of MEG, EEG, and invasive electrophysiological data. Comput Intell Neurosci. 2011;2011.
28. Franzmeier N, Buerger K, Teipel S, Stern Y, Dichgans M, Ewers M. Cognitive reserve moderates the association between functional network anticorrelations and memory in MCI. Neurobiol Aging. 2017;50.
29. de Oliveira DR, Lima MAA, Silva LRM, Ferreira DD, Duque CA. Second order blind identification algorithm with exact model order estimation for harmonic and interharmonic decomposition with reduced complexity. Int J Electr Power Energy Syst. 2021;125.
30. Tzourio-Mazoyer N, Landeau B, Papathanassiou D, Crivello F, Etard O, Delcroix N, et al. Automated anatomical labeling of activations in SPM using a macroscopic anatomical parcellation of the MNI MRI single-subject brain. NeuroImage. 2002;15(1).
31. Nolte G. The magnetic lead field theorem in the quasi-static approximation and its use for magnetoenchephalography forward calculation in realistic volume conductors. Phys Med Biol. 2003;48(22).
32. Van Veen BD, Van Drongelen W, Yuchtman M, Suzuki A. Localization of brain electrical activity via linearly constrained minimum variance spatial filtering. IEEE Trans Biomed Eng. 1997;44(9).
33. Bruns A, Eckhorn R, Jokeit H, Ebner A. Amplitude envelope correlation detects coupling among incoherent brain signals. Neuroreport. 2000;11(7).

34. Siems M, Pape AA, Hipp JF, Siegel M. Measuring the cortical correlation structure of spontaneous oscillatory activity with EEG and MEG. NeuroImage. 2016;129.
35. Zamm A, Debener S, Bauer AKR, Bleichner MG, Demos AP, Palmer C. Amplitude envelope correlations measure synchronous cortical oscillations in performing musicians. Ann N Y Acad Sci. 2018;1423(1).
36. Colclough GL, Woolrich MW, Tewarie PK, Brookes MJ, Quinn AJ, Smith SM. How reliable are MEG resting-state connectivity metrics? NeuroImage. 2016;138.
37. Schoonhoven DN, Briels CT, Hillebrand A, Scheltens P, Stam CJ, Gouw AA. Sensitive and reproducible MEG resting-state metrics of functional connectivity in Alzheimer's disease. Alzheimers Res Ther. 2022;14(1).
38. Brookes MJ, Woolrich MW, Barnes GR. Measuring functional connectivity in MEG: a multivariate approach insensitive to linear source leakage. NeuroImage. 2012;63(2):910–20.
39. Brookes MJ, Hale JR, Zumer JM, Stevenson CM, Francis ST, Barnes GR, et al. Measuring functional connectivity using MEG: methodology and comparison with fcMRI. NeuroImage. 2011;56(3):1082–104.
40. Brandes U, Pich C. Centrality Estimation in Large Networks *. Int J Bifurcat Chaos. 2007;17.
41. Maris E, Oostenveld R. Nonparametric statistical testing of EEG- and MEG-data. J Neurosci Methods. 2007;164(1):177–90.
42. Chuderski A. Fluid Intelligence and the Cross-Frequency Coupling of Neuronal Oscillations. Span J Psychol. 2016;19.
43. Vivekananda U, Bush D, Bisby JA, Baxendale S, Rodionov R, Diehl B et al. Theta power and theta-gamma coupling support long-term spatial memory retrieval. Hippocampus. 2021;31(2).
44. Hwang K, Hallquist MN, Luna B. The development of hub architecture in the human functional brain network. Cereb Cortex. 2013;23(10):2380–93.
45. Sporns O. Graph theory methods: applications in brain networks. Dialogues Clin Neurosci. 2018;20:111–21.
46. Damoiseaux JS, Prater KE, Miller BL, Greicius MD. Functional connectivity tracks clinical deterioration in Alzheimer's disease. Neurobiol Aging. 2012;33(4).
47. Cuesta P, Garcés P, Castellanos NP, López ME, Aurtenetxe S, Bajo R, et al. Influence of the APOE ε4 allele and mild cognitive impairment diagnosis in the disruption of the MEG resting state functional connectivity in sources space. J Alzheimer's Disease. 2015;44(2):493–505.
48. Davis SW, Dennis NA, Daselaar SM, Fleck MS, Cabeza R. Qué PASA? The posterior-anterior shift in aging. Cereb Cortex. 2008;18(5).
49. Zhang H, Lee A, Qiu A. A posterior-to-anterior shift of brain functional dynamics in aging. Brain Struct Funct. 2017;222(8).
50. Desgranges B, Mevel K, Chételat G, Eustache F. The default mode network in healthy aging and Alzheimer's disease. Int J Alzheimer's Disease. 2011.
51. Agosta F, Pievani M, Geroldi C, Copetti M, Frisoni GB, Filippi M. Resting state fMRI in Alzheimer's disease: beyond the default mode network. Neurobiol Aging. 2012;33(8).
52. Jones DT, Knopman DS, Gunter JL, Graff-Radford J, Vemuri P, Boeve BF, et al. Cascading network failure across the Alzheimer's disease spectrum. Brain. 2016;139(2):547–62.
53. Qi H, Liu H, Hu H, He H, Zhao X. Primary disruption of the memory-related subsystems of the Default Mode Network in Alzheimer's Disease: resting-state functional connectivity MRI study. Front Aging Neurosci. 2018;10.
54. Sperling RA, Dickerson BC, Pihlajamaki M, Vannini P, LaViolette PS, Vitolo OV et al. Functional alterations in memory networks in early alzheimer's disease. Vol. 12, NeuroMolecular Medicine. 2010.
55. Delbeuck X, Van Der Linden M, Collette F. Alzheimer's disease as a disconnection syndrome? Neuropsychol Rev. 2003;13(2):79–92.
56. Zhang HY, Wang SJ, Liu B, Ma ZL, Yang M, Zhang ZJ, et al. Resting brain connectivity: changes during the progress of Alzheimer disease. Radiology. 2010;256(2):598–606.
57. Paitel E R, Nielson K A. Cerebellar EEG source localization reveals age-related compensatory activity moderated by genetic risk for Alzheimer's disease. Psychophysiology. 2023;60(12):e14395.
58. Maestú F, de Haan W, Busche MA, DeFelipe J. Neuronal excitation/inhibition imbalance: core element of a translational perspective on Alzheimer pathophysiology. Ageing Research Reviews. Volume 69. Elsevier Ireland Ltd; 2021.
59. Garcia-Marin V, Blazquez-Llorca L, Rodriguez JR, Boluda S, Muntane G, Ferrer I, et al. Diminished perisomatic GABAergic terminals on cortical neurons adjacent to amyloid plaques. Front Neuroanat. 2009;3:28.
60. Busche MA, Hyman BT. Synergy between amyloid-β and tau in Alzheimer's disease. Volume 23. Nature Neuroscience. Nature Research; 2020. pp. 1183–93.
61. Stam CJ, De Haan W, Daffertshofer A, Jones BF, Manshanden I, Van Walsum C. AM. Graph theoretical analysis of magnetoencephalographic functional connectivity in Alzheimer's disease. Brain. 2009;132(1):213–24.
62. Wang R, Wang J, Yu H, Wei X, Yang C, Deng B. Decreased coherence and functional connectivity of electroencephalograph in Alzheimer's disease. Chaos. 2014;24(3).
63. Hata M, Kazui H, Tanaka T, Ishii R, Canuet L, Pascual-Marqui RD et al. Functional connectivity assessed by resting state EEG correlates with cognitive decline of Alzheimer's disease - an eLORETA study. Clin Neurophysiol. 2016;127(2).
64. Huang C, Wahlund LO, Dierks T, Julin P, Winblad B, Jelic V. Discrimination of Alzheimer's disease and mild cognitive impairment by equivalent EEG sources: a cross-sectional and longitudinal study. Clin Neurophysiol. 2000;111(11).
65. López ME, Aurtenetxe S, Pereda E, Cuesta P, Castellanos NP, Bruña R et al. Cognitive reserve is associated with the functional organization of the brain in healthy aging: A MEG study. Front Aging Neurosci. 2014;6(JUN).
66. Cabral J, Castaldo F, Vohryzek J, Litvak V, Bick C, Lambiotte R et al. Metastable oscillatory modes emerge from synchronization in the brain spacetime connectome. Commun Phys. 2022;5(1).
67. Engels MMA, Stam CJ, van der Flier WM, Scheltens P, de Waal H, van Straaten ECW. Declining functional connectivity and changing hub locations in Alzheimer's disease: an EEG study. BMC Neurol. 2015;15(1).
68. Siems M, Siegel M. Dissociated neuronal phase- and amplitude-coupling patterns in the human brain. Neuroimage. 2020;209:116538.
69. Koelewijn L, Bompas A, Tales A, Brookes MJ, Muthukumaraswamy SD, Bayer A, et al. Alzheimer's disease disrupts alpha and beta-band resting-state oscillatory network connectivity. Clin Neurophysiol. 2017;128(11):2347–57.
70. Traikapi A, Konstantinou N. Gamma Oscillations in Alzheimer's Disease and Their Potential Therapeutic Role. Front Syst Neurosci. 2021;15:782399.
71. Schmidtke K, Hermeneit S. High rate of conversion to Alzheimer's disease in a cohort of amnestic MCI patients. Int Psychogeriatr. 2008;20:96–108.
72. Dubois B, Albert ML. Amnestic MCI or prodromal Alzheimer's disease? 3, Lancet Neurol. 2004.

Publisher's note